The third robust synchronization method taught by Amoeba

Seido Nagano*

Department of Bioinformatics, Ritsumeikan University,

1-1-1 Nojihigashi, Shiga 525-8577, Japan

(Dated: November 22, 2023)

Abstract

Synchronization can produce dramatic changes in nature. Traditionally, two mathematical methods have been adopted to achieve such synchronization: The first method is to make the phase difference between oscillators, $\theta_i - \theta_j$, zero, and the second method is to make the oscillator variable difference, $x_i - x_j$, zero. However, in biological systems, the mechanism that realizes the above two methods has never been identified. Nevertheless, synchronization often plays an important role in many organisms. This indicates that there is a third way to achieve synchronization. Recently, such a method was discovered through the cellular dynamics study of a single-celled amoeba called *Dictyostelium discoideum*. This review details how *Dictyostelium discoideum* achieves synchronization at the molecular level and how it is mathematically generalized. Finally, we will apply the generalized synchronization method to various nonlinear systems.

Keywords: cellular slime mold, synchronization, receptor, limit cycle, nonlinearity, chemotaxis, cell-to-cell communication, diffusion

*Electronic address: nagano@sk.ritsumei.ac.jp

I. INTRODUCTION

In biology, synchronization[1][2][3] appears in many cases. For example, the maintenance of higher organisms, including humans, requires coordinated cell-cell and organ-to-organ interactions, and synchronization plays an essential role in such coordination. In addition, various frequencies have been observed in every biological system[4]. As a result, inter-frequency synchronization is also required. Biological synchronization is seemingly complex but its mechanism requires simplicity and robustness. It is because complexity of the mechanism increases system failure rate. Due to the above properties, biological systems are a good example for future innovation. However, due to evolution, various types of cells interact in multicellular systems, and it is quite difficult to elucidate the mechanism that achieves synchronization. For example, synchronization problems in the nervous system are being studied vigorously, and synchronization is perceived as essential for our proper brain activity. However, excessive synchronization causes a dysfunction called epilepsy[5], and due to the complexity of the central nervous system, its detailed mechanism remains an unsolved problem.

Fortunately, there is a very useful organism called *Dictyostelium discoideum* (Dicty)[6][7] for studying synchronization in biology. Dicty was first recognized by their Belousov-Zhabotinskii (BZ) reaction pattern in the aggregation of Dicty amoebas in 1983. Fig. 1 shows such a BZ pattern. BZ reaction is nonlinear chemical process[8]. Therefore, it was a great surprise that the same reaction pattern was observed in biology. By the help of the significant progress of the experimental techniques at the molecular and genetic level during the past 20 years, our understanding of Dicty has advanced and now our mathematical model can explain experimental observations consistently at the molecular level, too. In this review, we will explain it briefly and Dicty's synchronization scheme is mathematically simplified and generalized as the receptor-based synchronization (RBS) method for nonlinear oscillators.

First of all, we will briefly explain the survival strategy of Dicty as shown in Fig. 2. Dicty is unicellular amoeba, but when starved, many amoebas aggregate and form multicellular systems. Within aggregates, spores are formed. Spores can live long without food or water. In their aggregation process, 3',5'-cyclic adenosine monophosphate (cAMP), synthesized from adenosine triphosphate (ATP) by adenylate cyclase (AC), is periodically secreted ex-

FIG. 1: Belousov-Zhabotinskii reaction pattern in the aggregation of *Dictyostelium* amoebas (Newell, 1983). The light and dark bands arise from the different optical properties between moving and stationary amoebas. The cells look bright when moving and dark when stationary. The area is $6cm \times 8cm$.

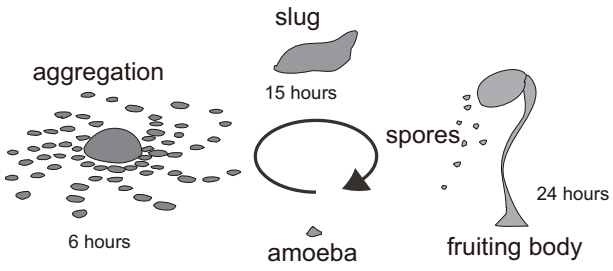

FIG. 2: Life cycle of *Dictyostelium discoideum* (Dicty). Dicty cells exist as free-living amoebas when food sources are available. However, when starved, Dicty amoebas aggregate into multicellular slags that eventually form fruiting bodies. After that, the spores that have fallen from the fruiting body germinate and become amoebas. It takes about 24 hours from aggregation to sporulation.

tracellularly. Usually, cAMP is a key molecule for intracellular signal transduction in every organisms and stays within cells.

What is unique about Dicty is that cAMP, which is used intracellularly in most living organisms, is also used for cell-cell communication. Since cAMP is commercially available, too, experimental control of cellular communication is also possible. Such a property is very helpful for the quantitative modeling study. The cAMP produced by the individual amoebas and secreted extracellularly form a circular diffusion field of cAMP that are superposed. Each amoeba surfs through the cAMP diffusion field in its denser direction, forming aggregates called slugs. ATP is essential for the survival of living things, as it is called the energy

currency of living things. On the other hand, cAMP, which is required for cell aggregation, is synthesized from ATP. Therefore, it is necessary to avoid overproduction of cAMP as much as possible for survival. If cell-cell synchronization of cAMP production is realized, large cAMP waves can be formed while suppressing ATP consumption in each cell. Amoeba aggregation must also be robust, as the external environment is not always ideal for proper cell movement. Therefore, studying Dicty can be a good first step in understanding the synchronization mechanism in biology.

II. DIFFUSION-ASSISTED AGGREGATION AND SYNCHRONIZATION [9][10][11]

Starved Dicty amoebas secrete extracellular cAMP and perform chemotactic movements towards the formation of aggregates called slags. Aggregation of Dicty amoebas requires the synthesis of cAMP from ATP, which is also required to sustain life, as it is called the energy currency of living things. Therefore, when ATP is exhausted, the amoebas die before the end of aggregation. Therefore, in order to save ATP as much as possible, the production of intracellular cAMP is stopped when the extracellular cAMP density is high, and the production of cAMP is resumed when the extracellular cAMP density is low. Such production regulation is performed by the cAMP receptor cAR1 (R in Fig. 3 (a)) in the cell membrane. However, there is a time lag between the detection of cAMP density and the start of cAMP production, and as shown in Fig. 4, cAMP production undergoes periodic fluctuations.

Fig. 3 (b) extracts only the key players from Fig. 3 (a). The experimentally confirmed more detailed molecular network[10] is briefly explained in Appendix. This section describes the Dicty strategy using the simplified scheme shown in Fig. 3 (b). First, assume that the intracellular cAMP density (P_j) and the cAMP receptor cAR1 (R_j) interact in the absence of extracellular secretion and satisfy the following equation:

$$\frac{dP_j^{in}}{dt} = F_j\left(P_j^{in}, R_j\right), \tag{1}$$

$$\frac{dR_j}{dt} = G_j\left(P_j^{in}, R_j\right), \tag{2}$$

where complex intracellular biochemical reactions are included within the functions of F_j and G_j, and P_j^{in} in $G_j\left(P_j^{in}, R_j\right)$ is the intracellular cAMP density detected by the cAMP re-

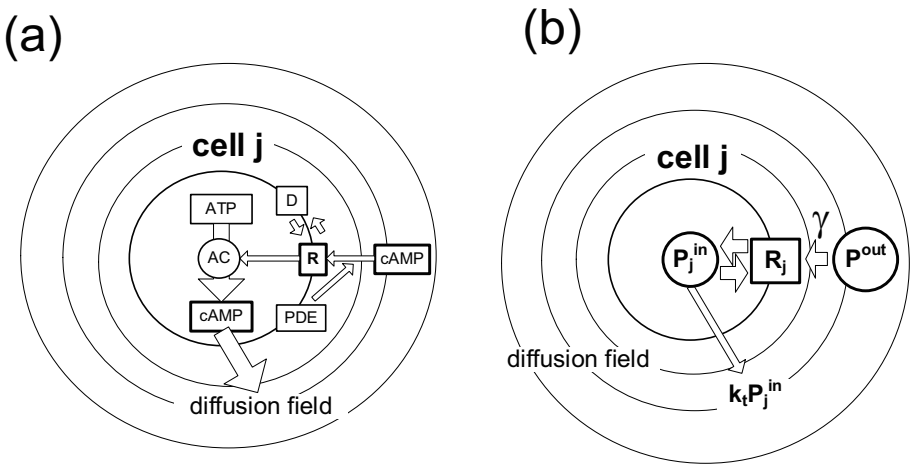

FIG. 3: (a) Control of cAMP synthesis and diffusion. Here, cAMP is synthesized from ATP by adenylate cyclase (AC) and secreted extracellularly with a leak rate of k_t. The synthesis of cAMP is regulated by the cAMP receptor (R). If the extracellular cAMP density is too high, the receptor changes to a desensitized state (D) and cAMP production ceases. (b) Schematic relationship between receptor R and product P. P^{in} is an intracellular product, and P^{out} is an extracellular diffusion field formed by products leaked from all cells, including itself.

ceptor. In addition, considering the properties of cAMP receptors, we assume that individual intracellular cAMP production processes constitute limit cycle oscillators.

When intracellular cAMP is secreted extracellularly with a leak rate of k_t, Eqs. (1) and (2) can be rewritten as follows.

$$\frac{dP_j^{in}}{dt} = F_j\left(P_j^{in}, R_j\right) - k_t P_j^{in}, \tag{3}$$

$$\frac{dR_j}{dt} = G_j\left(P_j^{in} + \gamma P_j^{out}, R_j\right), \tag{4}$$

where $P_j^{out} = P^{out}\left(\mathbf{r}_j, t\right)$ is extracellular cAMP density of cell j and γ is the sensitivity of the cAMP receptor. As a result, the net amount of cAMP recognized by the receptor in Eq. (2) becomes $P_j^{in} + \gamma P_j^{out}$ from P_j^{in}. Since the extracellular cAMP field is formed by the leaked cAMP from amoebas, $P^{out}\left(\mathbf{r}, t\right)$ is determined by the following diffusion equation[9]:

$$\frac{\partial P^{out}\left(\mathbf{r}, t\right)}{\partial t} = \sum_{j=1}^{N} k_t P_j^{in}\left(t\right)\delta\left(\mathbf{r} - \mathbf{r}_j\right) - k_d P^{out}\left(\mathbf{r}, t\right) + D\nabla^2 P^{out}\left(\mathbf{r}, t\right), \tag{5}$$

where D is the diffusion coefficient of cAMP, $\mathbf{r}_j$ is the positional vector of the j-th cell, δ is the two-dimensional delta function, and N is the total number of amoebas. Interestingly,

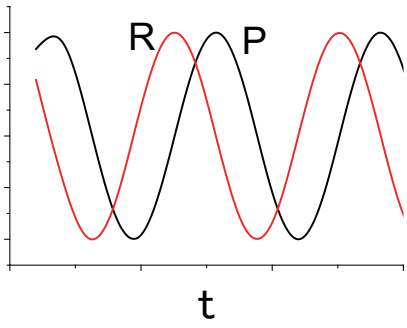

FIG. 4: A schematic periodic relationship between the activity of receptor R and the density of product P. As the activity of R increases, so does P. However, when P becomes too much, the activity of R decreases, and then P decreases. However, if P is too low, the activity of R increases again. Such changes are repeated in the virtual cell.

amoebas secrete not only cAMP, but also phosphodiesterase (PDE) which degrades cAMP. This corresponds to the term, $-k_d P^{out}(\mathbf{r}, t)$, and k_d is the dissociation rate of cAMP by PDE. This looks contradictory procedure. However, it plays an important role when extracellular environment is not ideal for the cAMP diffusion. If cAMP is not diffused properly, a dense cAMP field will always be maintained around the amoeba and cAMP production will stop. As a result, aggregation of amoebas fails. When D is large enough, PDE effect becomes negligible.

The amoeba movement in the cAMP diffusion field is determined by the following equation of motion[9]:

$$m_a \frac{d^2\mathbf{r}_j}{dt^2} = \epsilon_2 \nabla_j P^{out}(\mathbf{r}_j, t) - \sum_{i=1(i\neq j)}^{N} \nabla_j \phi_{m,n}(|\mathbf{r}_j - \mathbf{r}_i|) - \eta \frac{d\mathbf{r}_j}{dt}, \tag{6}$$

where m_a is the mass of one amoeba. On the right-hand side of Eq. (6), the first term is the chemotactic force, the second term is the cell-to-cell interaction force, and the last term is frictional force due to the substrate, and η is the friction coefficient. Fig. 5 shows several snap shots of the computer simulation.In this computer simulation, the intracellular molecular network in Appendix together with Eqs. (5) and (6) are adopted and the validity of our model has been experimentally confirmed[10].

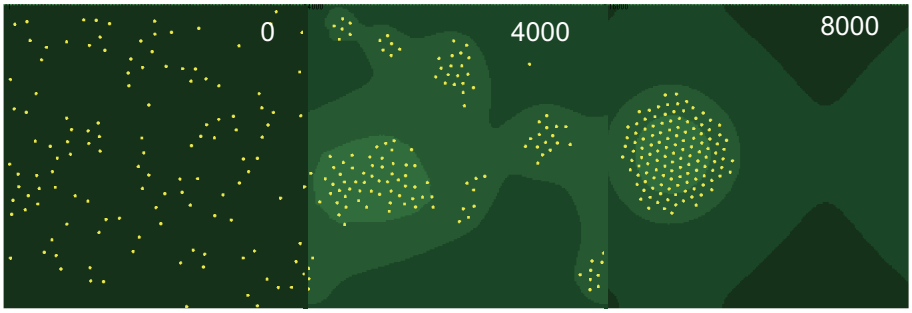

FIG. 5: Snap shots of the cellular dynamics simulation of *Dictyostelium discoideum*[10]. Closed yellow circles are *Dictyostelium* amoebas; brighter green color in the contour plots shows the higher extracellular cAMP density. Corresponding movie files can be found in the supplements of Reference [10].

III. RECEPTOR-BASED SYNCHRONIZATION (RBS) METHOD[12][13]

In this section, we elucidate the key synchronization mechanism from the aggregation of Dicty. First, we freeze the cellular motion. Next, we simplify the cAMP diffusion process as follows. The j-th cell receives cAMP form the i-th cell which is proportional to $k_t P_i^{in}$. As a result, total amount of cAMP which the j-th cell receives becomes

$$P_j^{out} = \sum_{i=1}^{N} \alpha_{ji} k_t P_i^{in}, \tag{7}$$

where α_{ji} are proportional constants. Then, Eq. (4) can be rewritten as

$$\frac{dR_j}{dt} = G_j \left(P_j^{in} + \gamma \sum_{i=1}^{N} \alpha_{ji} k_t P_i^{in}, R_j \right). \tag{8}$$

As a final step, we assume that the intracellular cAMP production rate is much larger than the its leakage rate, i.e., the condition $|F_j| \gg \left| k_t P_j^{in} \right|$ is satisfied. And, reading $\gamma \alpha_{ji} k_t$ as a redefined γ_{ji}, Eqs. (3) and (8) become

$$\frac{dP_j}{dt} = F_j \left(P_j, R_j \right), \tag{9}$$

$$\frac{dR_j}{dt} = G_j \left(P_j^R, R_j \right), \tag{10}$$

where

$$P_j^R = P_j + \sum_{i=1}^{N} \gamma_{ji} P_i. \tag{11}$$

For simplicity, P_j^{in} is read as P_j.

A. Application to van der Pol oscillators

One can apply the RBS method to the system of van der Pol oscillators as follows. The van der Pol equation is given by

$$\frac{d^2x_j}{dt^2} - \epsilon\left(1 - x_j^2\right)\frac{dx_j}{dt} + \omega_j^2 x_j = 0, \tag{12}$$

where ω_j is the natural frequency of the j-th oscillator and ϵ is the parameter that controls the degree of nonlinearity. Eq. (12) can be rewritten as

$$\frac{dx_j}{dt} = y_j \tag{13}$$

$$\frac{dy_j}{dt} = -\omega_j^2 x_j + \epsilon\left(1 - x_j^2\right) y_j. \tag{14}$$

As shown in Fig. 6, when applying the RBS method, there are two options: set (P_j, R_j) to (x_j, y_j) (Case 1) or (y_j, x_j) (Case 2).

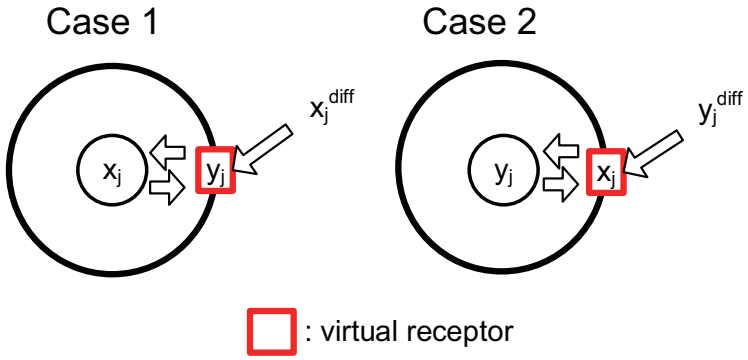

FIG. 6: Schematic view of the receptor-ligand coupling scheme for synchronization. Case 1: y_j is regarded as the activity of the virtual receptor, x_j and x_j^{diff} are the internal and the external stimuli, respectively, both of them are regarded as virtual ligands, and γ_j is the sensitivity of the receptor. Case 2: x_j is the activity of the virtual receptor, y_j and y_j^{diff} are the internal and the external stimuli, respectively, both of them are also regarded as virtual ligands. In both cases, it is assumed that two variables x_j and y_j constitute a limit cycle oscillator.

In Case 1, y_j is the activity of the virtual receptor and functional forms of F_j and G_j can

be derived from the following equations:

$$\frac{dx_j}{dt} = F_j\left(x_j, y_j\right) = y_j, \tag{15}$$

$$\frac{dy_j}{dt} = G_j\left(x_j, y_j\right) = -\omega_j^2 x_j + \epsilon\left(1 - x_j^2\right) y_j. \tag{16}$$

As a result, the coupled equations become

$$\frac{dx_j}{dt} = F_j\left(x_j, y_j\right) = y_j, \tag{17}$$

$$\frac{dy_j}{dt} = G_j\left(x_j^R, y_j\right) = -\omega_j^2 x_j^R + \epsilon\left[1 - \left(x_j^R\right)^2\right] y_j, \tag{18}$$

where

$$x_j^R = x_j + \gamma \sum_{i=1}^{N} x_i \equiv x_j + x_j^{diff}. \tag{19}$$

Fig.7 shows synchronization of two van der Pol oscillators in Case 1.

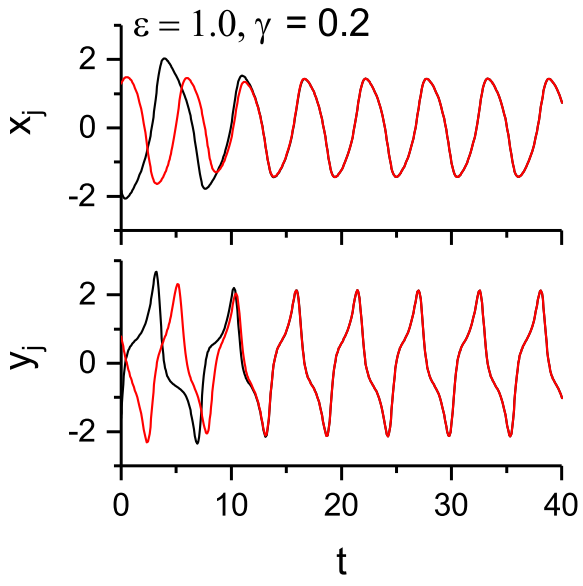

FIG. 7: Synchronization of two van der Pol oscillators in Case 1. Where $\omega_1 = \omega_2 = 1.0$.

In Case 2, x_j is the activity of the virtual receptor, and the roles of F and G are exchanged. Then coupled equations are:

$$\frac{dy_j}{dt} = F_j\left(y_j, x_j\right) = -\omega_j^2 x_j + \epsilon\left(1 - x_j^2\right) y_j, \tag{20}$$

$$\frac{dx_j}{dt} = G_j\left(y_j^R, x_j\right) = y_j^R, \tag{21}$$

where

$$y_j^R = y_j + \gamma \sum_{i=1}^{N} y_i \equiv y_j + y_j^{diff}. \tag{22}$$

Fig. 8 shows synchronization of two van der Pol oscillators in Case 2.

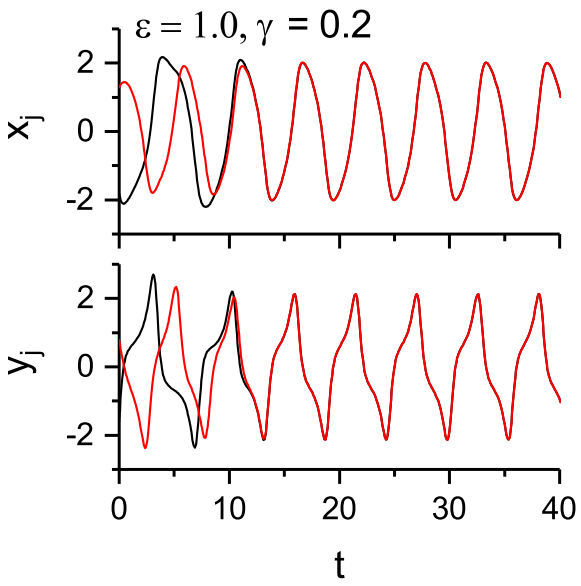

FIG. 8: Synchronization of two van der Pol oscillators in Case 2. Where $\omega_1 = \omega_2 = 1.0$.

Here we have shown only the case of two van der Pol oscillators because various cases including $N = 100$, and $\omega_1/\omega_2 = 100$ were studied in detail in Reference [13]. It was also confirmed that synchronization was always achieved under any initial condition.

The synchronized state is also the limit cycle state. In the synchronized state of Case 1, $x_1 = x_2 = \ldots = x_N \equiv x$ when $\omega_1 = \omega_2 = \ldots = \omega_N = \omega$. From Eq. (19), $x^R = (1 + N\gamma)\, x \equiv \alpha x$, and using Eqs. (17) and (18), we have

$$\frac{d^2x}{dt^2} - \epsilon \left[1 - \left(x^R\right)^2\right] \frac{dx}{dt} + \omega^2 x^R = 0. \tag{23}$$

With the product with α on both sides, we have

$$\frac{d^2x^R}{dt^2} - \epsilon \left[1 - \left(x^R\right)^2\right] \frac{dx^R}{dt} + \omega_s^2 x^R = 0, \tag{24}$$

where

$$\omega_s = \sqrt{\alpha}\omega = \sqrt{1 + N\gamma}\omega, \tag{25}$$

and $x = x^R/\alpha$. Eq. (24) shows that x^R is the solution of van der Pol oscillator with the intrinsic frequency ω_s. Furthermore, amplitudes of individual oscillators become smaller those of non-coupled van der Pol oscillators since $\alpha > 1$.

Similarly, in the synchronized state of Case 2, $y_1 = y_2 = \ldots = y_N \equiv y$ and $x_1 = x_2 = \ldots = x_N \equiv x$ when $\omega_1 = \omega_2 = \ldots = \omega_N = \omega$. From Eq. (22), $y^R = (1 + N\gamma)\, y \equiv \alpha y$, and with the product with α on both sides of Eq. (20), we have

$$\frac{d\,(\alpha y)}{dt} - \epsilon\left(1 - x^2\right)(\alpha y) + \alpha\omega^2 x = 0. \tag{26}$$

From Eq. (21), $dx/dt = y^R = \alpha y$. As a result, Eq. (26) can be written as

$$\frac{d^2x}{dt^2} - \epsilon\left(1 - x^2\right)\frac{dx}{dt} + \omega_s^2 x = 0. \tag{27}$$

However, the relationship between x and dx/dt becomes

$$y = \frac{1}{\alpha}\frac{dx}{dt} = \frac{1}{(1 + N\gamma)}\frac{dx}{dt}. \tag{28}$$

This means that in both Case 1 and Case 2, the globally synchronized state of the van der Pol oscillator system is also in the limit cycle state, and the synchronized state of the RBS model is very robust.

When the intrinsic frequencies of all oscillators are not equal, it was numerically found that

$$\omega_s = \left[\omega_a^2 + \gamma \sum_{i=1}^{N} \omega_i^2\right]^{1/2} \tag{29}$$

is a good approximation[13]. Where $\omega_a = Max\,(\omega_1, \omega_2, ..., \omega_N)$.

Frequency to amplitude modulation. The value of the coupling constant γ controls the efficiency of synchronization. Fig. 9 shows the inter-frequency synchronization of van der Pol oscillators in Case 1. An interesting point is that the frequency difference is converted to the amplitude difference in the synchronized state. Frequency to amplitude modulation in Case 2 is shown in Fig. 10.

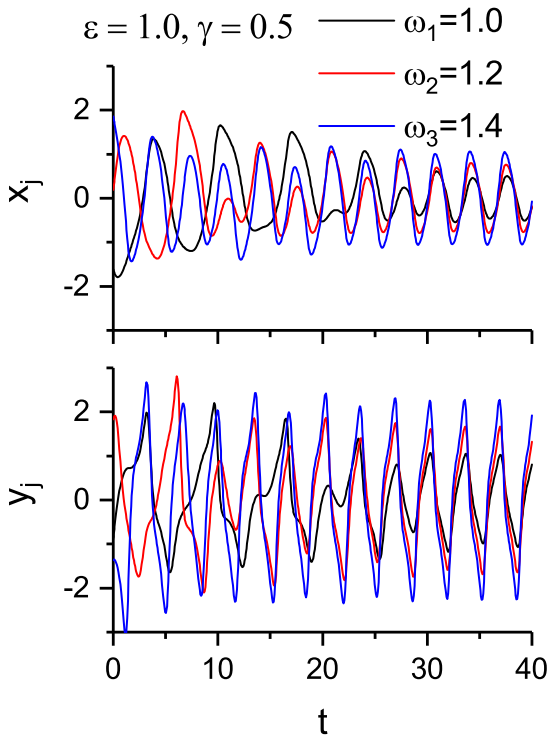

FIG. 9: Frequency to amplitude modulation of van der Pol oscillators in Case 1. Amplitudes of x_j is nearly proportional to ω_j^2.

B. Application to Rayleigh oscillators

As the second example, we apply the RBS method to Rayleigh oscillators. The equation for the Rayleigh oscillator is

$$\frac{d^2x_j}{dt^2} - \epsilon\left[1 - \frac{1}{3}\left(\frac{dx_j}{dt}\right)^2\right]\frac{dx_j}{dt} + \omega_j^2 x_j = 0, \tag{30}$$

and the above equation can be rewritten as

$$\frac{dx_j}{dt} = F_j\left(x_j, y_j\right) = y_j, \tag{31}$$

$$\frac{dy_j}{dt} = G_j\left(x_j, y_j\right) = -\omega_j^2 x_j + \epsilon\left(1 - \frac{1}{3}y_j^2\right)y_j. \tag{32}$$

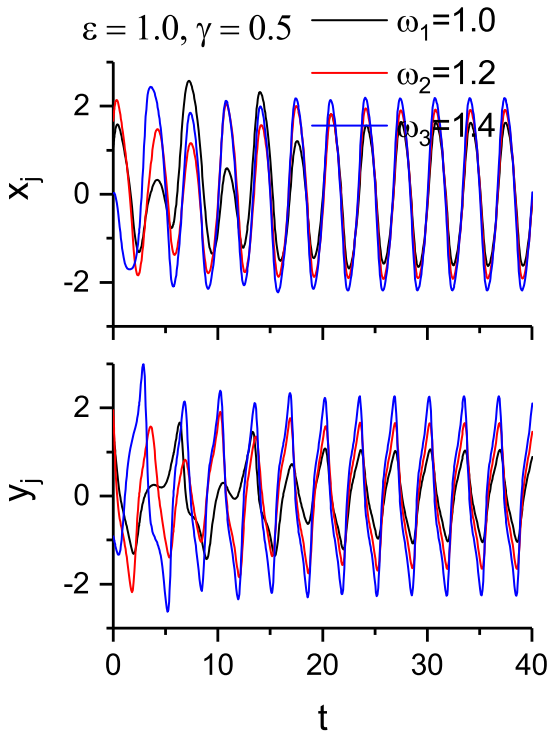

FIG. 10: Frequency to amplitude modulation of van der Pol oscillators in Case 2. Amplitudes of y_j is nearly proportional to ω_j^2.

As a result, in Case 1, y_j is the activity of the virtual receptor and the coupled equations become

$$\frac{dx_j}{dt} = F_j\left(x_j, y_j\right) = y_j, \tag{33}$$

$$\frac{dy_j}{dt} = G_j\left(x_j^R, y_j\right) = -\omega_j^2 x_j^R + \epsilon\left(1 - \frac{1}{3}y_j^2\right) y_j, \tag{34}$$

where

$$x_j^R = x_j + \gamma \sum_{i=1}^{N} x_i. \tag{35}$$

Fig. 11 shows in-phase synchronization of two Rayleigh oscillators. However, as shown in Fig. 12 anti-phase synchronization appears when the initial condition is close to the ant-phase state.

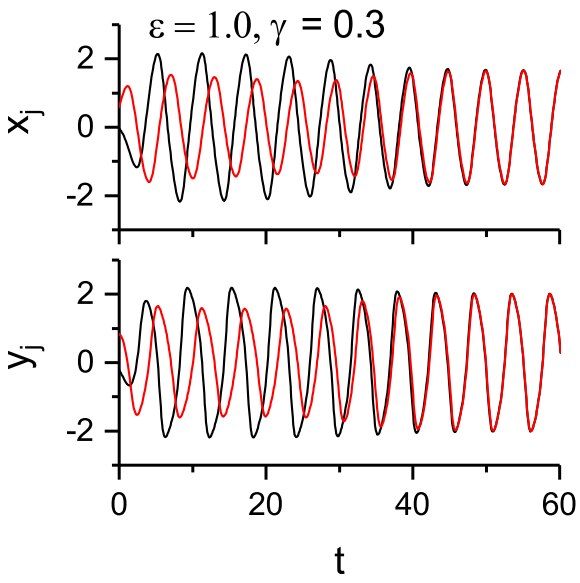

FIG. 11: In-phase synchronization of two Rayleigh oscillators.

Similarly to Case 1, the coupled equations in Case 2 become

$$\frac{dy_j}{dt} = F_j\left(y_j, x_j\right) = -\omega_j^2 x_j + \epsilon\left(1 - \frac{1}{3}y_j^2\right) y_j, \tag{36}$$

$$\frac{dx_j}{dt} = G_j\left(y_j^R, x_j\right) = y_j^R, \tag{37}$$

where

$$y_j^R = y_j + \gamma \sum_{i=1}^{N} y_i. \tag{38}$$

In this case too, anti-phase synchronization appears when the initial condition is close to the ant-phase state.

For Rayleigh oscillators, both in-phase synchronization and anti-phase synchronization were seen depending on the initial conditions. However, when Case 1 and Case 2 are mixed, only in-phase synchronization was observed as shown in Fig. 13. That is, in oscillator 1, y_1 is the virtual receptor and x_2 is the virtual receptor in oscillator 2. As a result, the

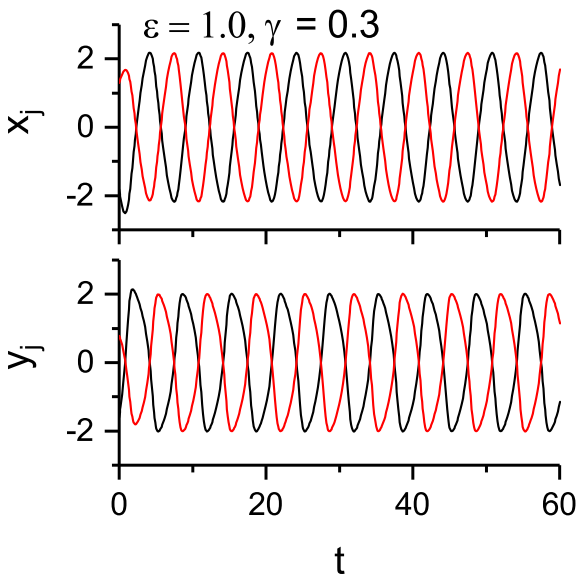

FIG. 12: Anti-phase synchronization of two Rayleigh oscillators. Please note that the initial condition here is different from that in Fig. 11.

simultaneous equations are:

$$\frac{dx_1}{dt} = y_1, \tag{39}$$

$$\frac{dy_1}{dt} = -\omega_1^2 x_1^R + \epsilon\left(1 - \frac{1}{3}y_1^2\right) y_1, \tag{40}$$

$$\frac{dy_2}{dt} = -\omega_2^2 x_2 + \epsilon\left(1 - \frac{1}{3}y_2^2\right) y_2, \tag{41}$$

$$\frac{dx_2}{dt} = y_2^R, \tag{42}$$

where

$$x_1^R = x_1 + \gamma\left(x_1 + y_2\right), \tag{43}$$

$$y_2^R = y_2 + \gamma\left(y_2 + x_1\right). \tag{44}$$

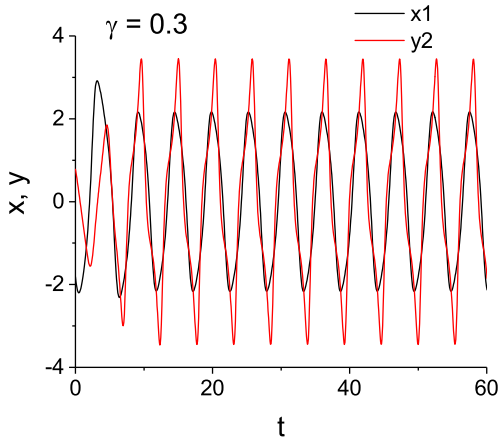

FIG. 13: In the case of Rayleigh oscillators in which Case 1 and Case 2 are mixed, only in-phase synchronization can be achieved under any initial conditions.

C. Application to Brusselators

As a final final example, we apply the RBS method to Brusselators. The equation for the Brusselator is given by

$$\frac{dx_j}{dt} = F_j(x_j, y_j) = a - (b+1)\,x_j + x_j^2 y_j, \tag{45}$$

$$\frac{dy_j}{dt} = G_j(x_j, y_j) = b x_j - x_j^2 y_j, \tag{46}$$

where $a = 1.0$, $b = 2.1$. As a result, in Case 1, y_j is the activity of the virtual receptor and the coupled equations become

$$\frac{dx_j}{dt} = F_j(x_j, y_j) = a - (b+1)\,x_j + x_j^2 y_j,, \tag{47}$$

$$\frac{dy_j}{dt} = G_j\left(x_j^R, y_j\right) = b x_j^R - \left(x_j^R\right)^2 y_j, \tag{48}$$

where

$$x_j^R = x_j + \gamma \sum_{i=1}^{N} x_i. \tag{49}$$

Fig. 14 shows synchronization of two Brusselators. When γ value is small, both anti-phase synchronization in-phase synchronization appear, but only in-phase synchronization is observed when γ value is increased. However, amplitudes of the synchronized state is significantly reduced.

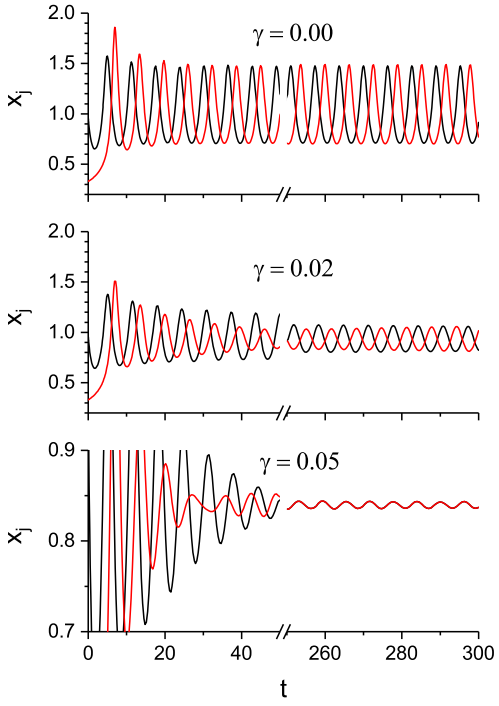

FIG. 14: In-phase synchronization and anti-phase synchronization of two Brusselators in Case 1. For $\gamma = 0.05$, only in-phase synchronization is observed. However, the amplitude becomes extremely small.

Similarly to Case 1, the coupled equations in Case 2 become

$$\frac{dy_j}{dt} = F_j\left(y_j, x_j\right) = bx_j - x_j^2 y_j, \tag{50}$$

$$\frac{dx_j}{dt} = G_j\left(y_j^{R,} x_j\right) = a - (b+1)\, x_j + x_j^2 y_j^R, \tag{51}$$

where

$$y_j^R = y_j + \gamma \sum_{i=1}^{N} y_i. \tag{52}$$

As shown in Fig. 15, this case also shows similar characteristics of synchronization to Case 1.

D. Application to the mixed oscillator systems

Here, we apply the RBS method to the following two cases of the mixed oscillator systems. The first case is the coupled system of the van der Pol oscillator and Rayleigh oscillator.

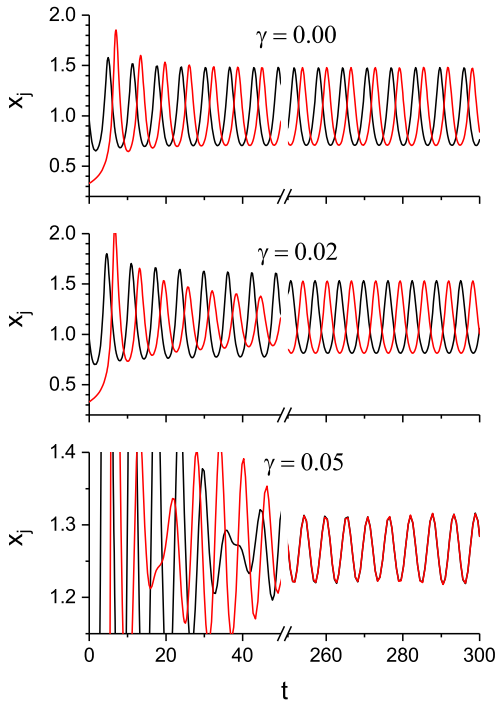

FIG. 15: In-phase synchronization and anti-phase synchronization of two Brusselators in Case 2. For $\gamma = 0.05$, only in-phase synchronization is observed. However, the amplitude becomes extremely small.

The corresponding equations become

$$\frac{dx_1}{dt} = y_1 \tag{53}$$

$$\frac{dy_1}{dt} = -\omega^2 x_1^R + \epsilon\left[1 - \left(x_1^R\right)^2\right] y_1, \tag{54}$$

$$\frac{dx_2}{dt} = y_2, \tag{55}$$

$$\frac{dy_2}{dt} = -\omega^2 x_2^R + \epsilon\left(1 - \frac{1}{3}y_2^2\right) y_2, \tag{56}$$

where

$$x_1^R = x_1 + \gamma\left(x_1 + x_2\right), \tag{57}$$

$$x_2^R = x_2 + \gamma\left(x_1 + x_2\right). \tag{58}$$

Fig. 16 shows that synchronization can be achieved by increasing the frequency of the synchronized state.

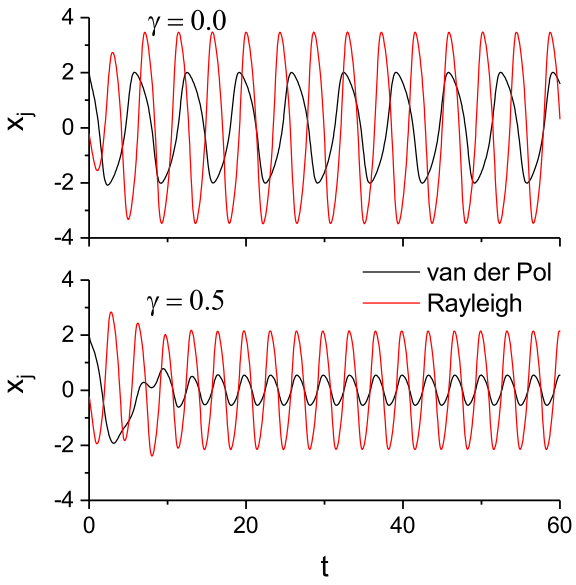

FIG. 16: Synchronization between van der Pol oscillator and Rayleigh oscillator. Where the intrinsic frequency of the van der Pol oscillator is $\omega = 1.0$.

The second case is the coupled system of the van der Pol oscillator and Brusselator. The corresponding equations become

$$\frac{dx_1}{dt} = y_1 \tag{59}$$

$$\frac{dy_1}{dt} = -\omega^2 x_1^R + \epsilon\left[1 - \left(x_1^R\right)^2\right] y_1, \tag{60}$$

$$\frac{dx_2}{dt} = a - (b+1)\, x_2 + x_2^2 y_2, \tag{61}$$

$$\frac{dy_2}{dt} = b x_2^R - \left(x_2^R\right)^2 y_2, \tag{62}$$

where

$$x_1^R = x_1 + \gamma\,(x_1 + x_2)\,, \tag{63}$$

$$x_2^R = x_2 + \gamma\,(x_1 + x_2)\,. \tag{64}$$

In this case, too, successful synchronization is shown in Fig. 17. The frequency of the synchronized state is also increased.

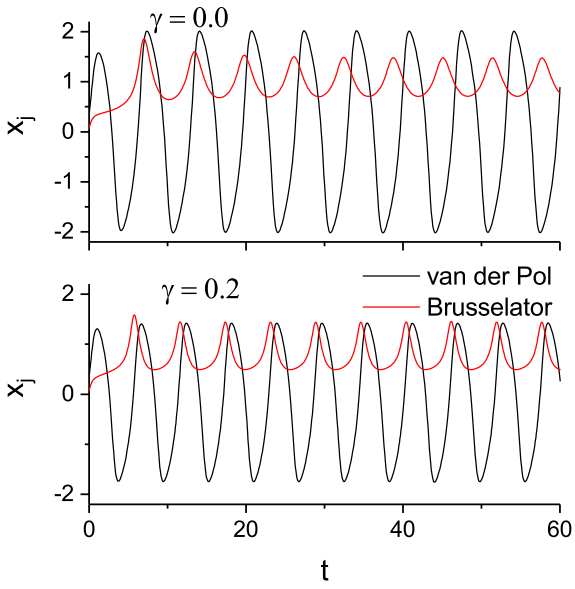

FIG. 17: Synchronization between van der Pol oscillator and Brusselator. Where the intrinsic frequency of the van der Pol oscillator is $\omega = 1.0$.

E. Properties of the global synchronization

In this section, we have applied the RBS method to various coupled nonlinear oscillator systems. As a result, two types of properties in the synchronized state were clarified. One is the change in frequency. The frequency under synchronization is always higher than the frequency of each uncoupled oscillator. The other is the change in amplitude. The amplitude of the synchronous state is smaller than the amplitude of each uncoupled oscillator. That is, the RBS method achieves global synchronization by changing both frequency and amplitude. This is very different from the traditional methods.

Amplitude reduction is a very important property in Dicty. If the number of amoebas is large enough, the amplitude of the cAMP wave sent out from the aggregate will be extremely small. This means that the cAMP density gradient also disappears. As a result, the further aggregation of amoeba due to chemotaxis stops. This means that amplitude reduction is used to count the number of amoebas in the aggregate.

The RBS method introduces a non-linear coupling between the non-linear oscillators by means of a virtual receptor. Therefore, in the RBS method, it is considered that the relative strength between the non-linearity in each oscillator and the non-linearity in the interaction

produces various synchronization states.

IV. EXTERNAL SYNCHRONIZATION OF MUTUALLY COUPLED OSCILLATORS[14][15]

Here, consider the case where a periodic external field is added to a synchronous system that is interconnected with each other as shown in Fig. 18. The main focus of this section is external control without losing synchronization within the coupled system. One of the most typical cases in biology is circadian rhythm. The strong sunlight can reset the activity of the biological system without breaking the order in the living body. Question is how such external control can be realized mathematically. This problem can be handled by

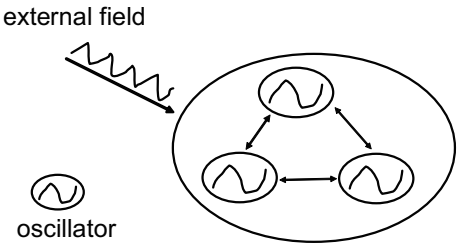

FIG. 18: Mutually coupled oscillators in the presence of oscillatory external field.

the RBS method as follows[14]. First of all, we assume that the external oscillatory field $f^{out}(t) = A \sin \omega_0 t$ is applied when $t_0 \leqq t \leqq t_1$. In this case we rewrite Eq. (10) as

$$\frac{dP_j}{dt} = F_j(P_j, R_j), \tag{65}$$

$$\frac{dR_j}{dt} = G_j\left(P_j^R, R_j\right) + f^{out}, \tag{66}$$

where

$$P_j^R = P_j + \sum_{i=1}^{N} \gamma_{ji} P_i. \tag{67}$$

Here it is assumed that the virtual receptor receives the external field independently from the mutual coupling between oscillators. Validity of this assumption was confirmed by the coupled van der Pol oscillator systems[14]. Here too, there are two choices whether the virtual receptor is y_j or x_j. When y_j is the virtual receptor (Case 1), we adopt

$$\frac{dx_j}{dt} = F_j(x_j, y_j) = y_j, \tag{68}$$

$$\frac{dy_j}{dt} = G_j\left(x_j^R, y_j\right) = -\omega_j^2 x_j^R + \epsilon\left[1 - \left(x_j^R\right)^2\right] y_j + f^{out}, \tag{69}$$

where

$$x_j^R = x_j + \gamma \sum_{i=1}^{N} x_i. \tag{70}$$

On the other hand, when x_j is the virtual receptor (Case 2), we have

$$\frac{dy_j}{dt} = F_j\left(y_j, x_j\right) = -\omega_j^2 x_j + \epsilon\left(1 - x_j^2\right) y_j, \tag{71}$$

$$\frac{dx_j}{dt} = G_j\left(y_j^R, x_j\right) = y_j^R + f^{out}, \tag{72}$$

where

$$y_j^R = y_j + \gamma \sum_{i=1}^{N} y_i. \tag{73}$$

Fig. 19 shows that a periodic external field can provide external control without breaking synchronization between oscillators. Here, the natural frequency of the van der Pol oscillator and the frequency of the external field are intentionally set differently. Even in such cases, the external field can change the frequency of the coupled system without breaking the synchronization state. What's more, turning off external fields immediately reverts to the previous sync state.

As the next test, a periodic external field was applied to the anti-phase-locked state. Fig. 20 shows that the anti-phase synchronization state between Rayleigh oscillators can be changed to the in-phase synchronization state by the oscillating external field. What's even more interesting is that the in-phase synchronization is maintained even when the external field is turned off. Similarly, Fig. 21 shows that anti-synchronized state of Brusselators can be changed to the in-phase synchronized state by the oscillatory external filed.

We have investigated another way[15] to introduce the external filed into the RBS method. In that case, instead of Eqs (65)-(67), the following equations were adopted. Namely,

$$\frac{dP_j}{dt} = F_j\left(P_j, R_j\right), \tag{74}$$

$$\frac{dR_j}{dt} = G_j\left(P_j^R, R_j\right), \tag{75}$$

where

$$P_j^R = P_j + \sum_{i=1}^{N} \gamma_{ji} P_i + f^{out}. \tag{76}$$

This generalization worked well when the system had only one single oscillator[15]. Also, when the external frequency was increased, the previously observed M: N synchronization[4]

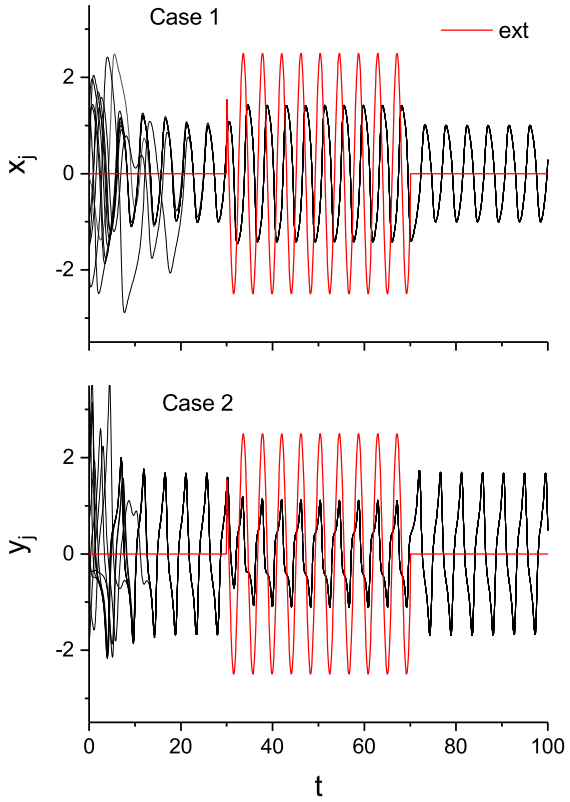

FIG. 19: External control of the synchronized state of 10 van der Pol oscillators, where intrinsic frequency $\omega_j = 1.0$ and the external frequency $\omega_{ext} = 1.5$.

did not appear, only 1: 1 synchronization was observed. On the other hand, in the case of a coupled oscillator system, the coupling between the oscillators and the external oscillatory field compete with each other in Eq. (76). As a result, the mutual synchronization was broken by the external oscillatory field. This shows the limits of the above two-variable model. However, although not covered in this review, the three-variable model introduced to solve the problem of noise reduction in chemotaxis[16] did not show this problem.

V. DIFFUSION AND SYNCHRONIZATION

In the 17th century, Huygens discovered that two pendulum clocks hanging on the same beam were in sync. Recently, it was found that two pendulum metronomes on a light, easily movable platform can be synchronized and anti-phase synchronization was also observed

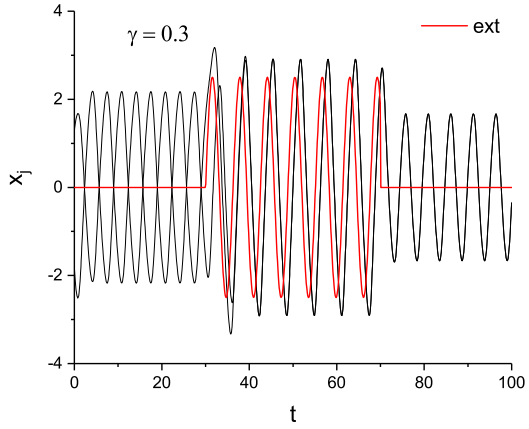

FIG. 20: The anti-phase synchronized state of Rayleigh oscillators in Figure 12 is changed to the in-phase synchronized state by the periodic external field.

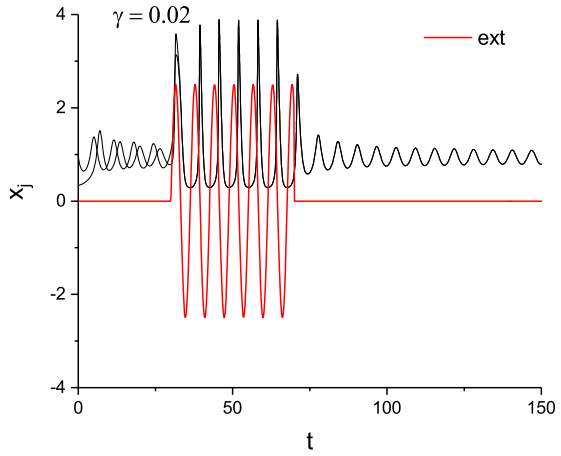

FIG. 21: The anti-phase synchronized state of Brusselators in Fig. 15 can be changed to the in-phase synchronized state by the periodic external field.

under special conditions [17]. There are important similarities between the above two cases and the current RBS method. The periodic movement of the pendulum creates small periodic vibrations around the pendulum clock or metronome and propagates over the beam or platform like a diffuse field that decays with distance. The diffuse field of the superimposed vibrations is the noise itself for the individual periodic motions of the pendulum clock and

metronome. The noise disturbs the periodic motion to some extent. However, pendulum clocks and metronomes have a characteristic like a limit cycle that returns to periodic motion. The motion to return to the periodic motion continues until the diffusion field of vibration is not recognized as noise. The destination is the mutual synchronization state. The diffusion field of vibration is also synchronized there, and it is no longer recognized as noise. This is exactly the RBS method itself. In the case of Dicty, cAMP is secreted extracellularly from individual amoebas to form a diffusion field of cAMP, which acts as noise for limit cycle intracellular cAMP production via receptors. However, as the whole synchronization is realized, the cAMP diffusion field is not recognized as noise and a new steady periodic motion state is realized. In principle, the above three cases are the same.

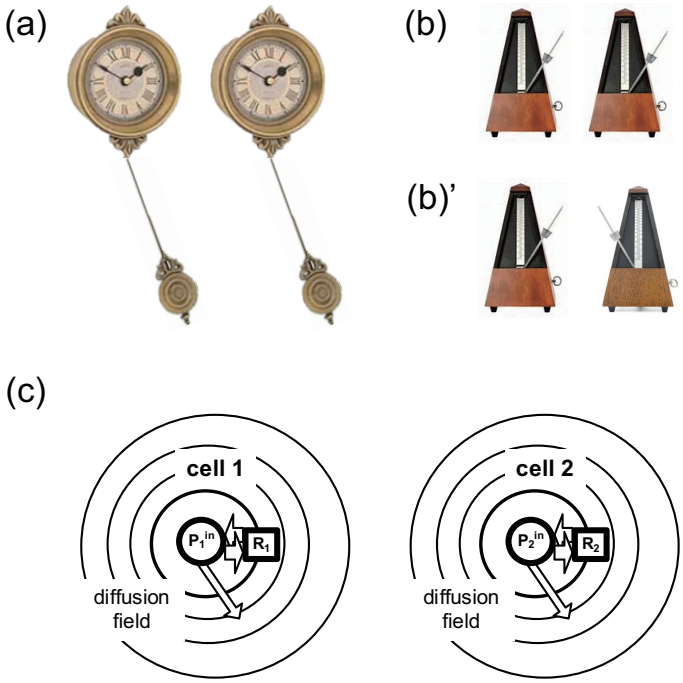

FIG. 22: The role of the diffusion in the synchronization. (a) Pendulum clock synchronization, (b) Metronome synchronization, (b)' Metronome anti-phase synchronization, (c) *Dictyostelium discoideum*.

A similar phenomenon can be seen in the formation of snowflakes. The crystal structure of snowflakes is much larger than the characteristic distance of intermolecular interactions. Nevertheless, a regular and complex structure is realized. In this case, we can assume as follows[18]. Water molecules generate small damped waves in the air due to Stokes friction. The waves in the air produced by many water molecules overlap to form a long-distance

force, which contributes to the formation of a macroscopic ordered structure that exceeds the range of intermolecular force. This is the same as the aggregation strategy of Dicty. Dicty amoebas intentionally create long-distance interactions by secreting and spreading cAMP extracellularly.

VI. SUMMARY

The main difficulty in studying biological systems is the large number of molecular and cellular types that work together in living organisms. As a result, quantitative research in biology is generally a daunting task. Fortunately, Dicty could solve the above difficulties. In addition, the communication molecule between amoebas is cAMP, which is one of two well-known messenger molecules in any cell. As a result, large quantities of cAMP are commercially available. The fact that extracellular cAMP secretion is extremely rare makes Dicty a very valuable organism for quantitative studies of biology. Genetically, too, it has become possible to change the effect of the target molecule in the molecular network shown in Fig. A-1. By comparing the experimentally observed patterns with the cellular dynamics simulation studies, we were able to confirm the validity of the theoretical model shown in the Appendix.

It is sure that unique properties of Dicty enabled us to elucidate the key mechanism to achieve synchronization, and mathematically generalize it as the RBS method. Mathematical generalization of the receptor dynamics is also very meaningful because receptor-ligand interactions are very important regulatory players in biology.

It is easy to recognize the synchronized state by the condition whether the phase difference $\theta_i - \theta_j$ is zero, or the oscillator variable difference $x_i - x_j$ is zero. It is also easy to set up mathematically the synchronization problem based on the phase or the oscillator variable. As a result, such schemes have dominated the synchronization study for a long time. The major difference between the RBS method and the above two methods is that the superposition of the oscillator variables $x_i + x_j$ achieves synchronization with the help of receptor dynamics. Also, synchronization is achieved even if $x_i \neq x_j$. Superposition of diffusion fields from individual signal sources is common in biology. Therefore, widespread application of the RBS method in biology can be expected in the future.

In the real world, we can not escape from the noise. Even for Dicty, there is a problem of

small signal-to-noise ratio for the chemotactic movement of Dicty. For such a case, receptor-receptor interaction becomes important. We hope interested readers see Reference [16].

Similarly, neural synchronization was not taken up in this review. Ion channels on the cell surface are also considered to be a type of receptor in abroad sense. Recently, we have successfully generalized the RBS model to neurons as the ion-channel based synchronization method. For neural synchronization, we hope readers see Reference [19]. As a result, it has confirmed again that the receptor dynamics is very important in the biological synchronization in general.

Acknowledgments

We would like to thank Dr. Shunsuke Sakurai and Dr. Atsushi Yokoyama for their valuable collaboration.

Appendix A: The molecular network of *Dictyostelium discoideum*[10][11]

Experimentally confirmed molecular network[10] is shown in Fig. 23.

Receptor dynamics and G protein dynamics can be written as:

$$\mathrm{cAMP}_e + \mathrm{cAR1} \underset{k_{14}}{\overset{k_{13}}{\rightleftarrows}} \mathrm{cAMP}_e \cdot \mathrm{cAR1} \equiv \mathrm{cAR1}^A, \tag{A1}$$

$$\mathrm{G} \underset{k_{16}}{\overset{k_{15}\left[\mathrm{cAR1}^A\right]}{\rightleftarrows}} \mathrm{G}_\alpha + \mathrm{G}_{\beta\gamma}, \tag{A2}$$

where G denotes the inactive G-protein and $\mathrm{cAR1}^A$ is the active, ligand-bound cAR1 receptor. Below are the conservation laws for cAR1 and G-protein,

$$[\mathrm{cAR1}] + \left[\mathrm{cAR1}^A\right] = \mathrm{cAR1}_0 = \mathrm{G}_0, \tag{A3}$$

$$[\mathrm{G}] + [\mathrm{G}_\alpha] = \mathrm{G}_0, \tag{A4}$$

where G_0 and $\mathrm{cAR1}_0$ are total density of G-protein and that of cAR1. It is also assumed that the total number of G-proteins is equal to the the total number of receptors, and the relationship $[G_\alpha] = [G_{\beta\gamma}]$ is maintained. The expression $[A]$ represents the density of the molecule A.

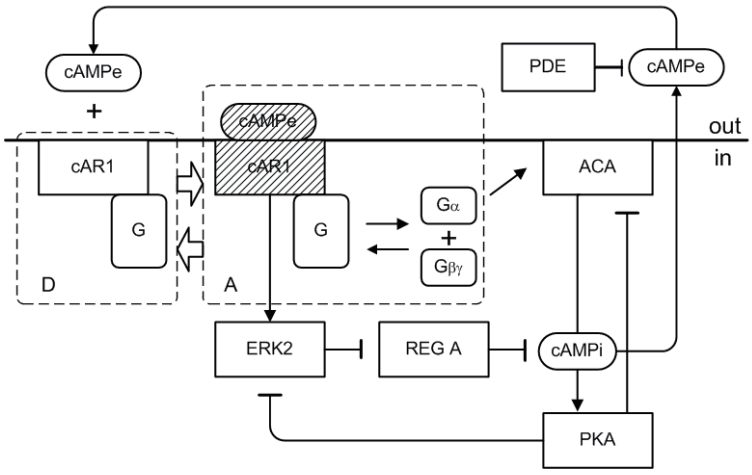

FIG. 23: A molecular network for spontaneous cAMP oscillations and adaptation. Extracellular cAMP (cAMPe) binds cAMP receptors (cAR1), which promotes dissociation of G_α subunit from G-protein, and G_α activates intracellular cAMP production by ACA. Once the density of G_α is sufficiently increased within the cell, cAMP production is halted, leading to the adaptation and desensitization of the receptors.

The molecular network in Fig. 23 can be expressed as

$$\frac{d\left[\mathrm{ACA}\right]}{dt} = k_1\left[\mathrm{G}_\alpha\right] - k_2\left[\mathrm{PKA}\right]\left[\mathrm{ACA}\right], \tag{A5}$$

$$\frac{d\left[\mathrm{PKA}\right]}{dt} = k_3\left[\mathrm{cAMPi}\right] - k_4\left[\mathrm{PKA}\right], \tag{A6}$$

$$\frac{d\left[\mathrm{ERK2}\right]}{dt} = k_5\left[\mathrm{cAR1}^A\right] - k_6\left[\mathrm{PKA}\right]\left[\mathrm{ERK2}\right], \tag{A7}$$

$$\frac{d\left[\mathrm{RegA}\right]}{dt} = k_7 - k_8\left[\mathrm{ERK2}\right]\left[\mathrm{RegA}\right], \tag{A8}$$

$$\frac{d\left[\mathrm{cAMPi}\right]}{dt} = k_9\left[\mathrm{ACA}\right] - k_{10}\left[\mathrm{RegA}\right]\left[\mathrm{cAMPi}\right], \tag{A9}$$

$$\frac{d\left[\mathrm{cAMPe}\right]}{dt} = k_{11}\left[\mathrm{cAMPi}\right] - k_{12}\left[\mathrm{cAMPe}\right], \tag{A10}$$

$$\frac{d\left[\mathrm{cAR1}^A\right]}{dt} = k_{13}\left(\mathrm{G}_0 - \left[\mathrm{cAR1}^A\right]\right)\left[\mathrm{cAMPe}\right] - k_{14}\left[\mathrm{cAR1}^A\right], \tag{A11}$$

$$\frac{d\left[\mathrm{G}_\alpha\right]}{dt} = k_{15}\left[\mathrm{cAR1}^A\right]\left(\mathrm{G}_0 - \left[\mathrm{G}_\alpha\right]\right) - k_{16}\left[\mathrm{G}_\alpha\right]^2, \tag{A12}$$

where k_i are numerical constants. A numerical simulation result of the above molecular dynamics is shown in Fig. 24. See Reference [10] for more information.

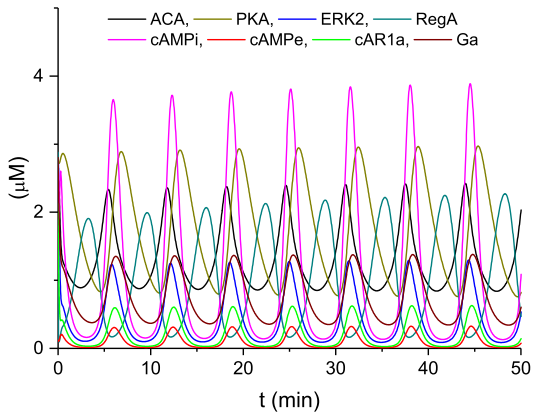

FIG. 24: The limit cycle dynamics of molecules in Fig. 23.

[1] A. Goldbeter, *Biochemical oscillations and cellular rhythms: the molecular bases of periodic and chaotic behaviour*, Cambridge University Press, 1996.

[2] S.H. Strogatz, *Nonlinear dynamics and chaos: With applications to physics, biology, chemistry, and engineering*, Westview Press, 1994.

[3] A. Pikovsky, M. Rosenblum, and J. Kurths, *Synchronization: a universal concept in nonlinear sciences*, Cambridge University Press, 2001.

[4] L. Glass and M.C. Mackey, *From clocks to chaos* ,Princeton University Press, 1988.

[5] P. Jiruska, M. De Curtis, J.G. Jefferys, C.A. Schevon, S.J. Schiff,, and K. Schindler, "Synchronization and desynchronization in epilepsy: controversies and hypotheses", *The Journal of physiology*, **591**, 787-797, 2013.

[6] R. H. Kessin and F. Jakob, *Dictyostelium : evolution, cell biology, and the development of multicellularity*, Cambridge University Press, Cambridge, 2001.

[7] S. Nagano, "Modeling the model organism *Dictyostelium discoideum*", *Develop. Growth Differ.*, **42** 541, 2000.

[8] L. Edelstein-Keshet, *Mathematical models in biology*, SIAM, 2005.

[9] S. Nagano, "Diffusion-Assisted Aggregation and Synchronization in *Dictyostelium discoideum*", *Phys Rev Lett* **80**, 4826-4829, 1998.

[10] S. Nagano and S. Sakurai, "Cell-to-cell coordination for the spontaneous cAMP oscillation in *Dictyostelium*", *Phys Rev E*, **88**, 062710, 2013.

[11] S. Sakurai, and S. Nagano, "A molecular network underlying spontaneous cAMP oscillation and synchronization in *Dictyostelium*", *J. theor. Biology*, **307**, 37-41, 2012.

[12] S. Nagano, "Receptor-Product Coupling Scheme for Synchronization", *Prog Theor Phys*, **103**, 229-244, 2000.

[13] S. Nagano, "Biological Receptor Scheme for the Robust Synchronization of Limit Cycle Oscillators", *Prog Theor Phys*, **107**, 861-877, 2002.

[14] A. Yokoyama and S. Nagano, "Biological Receptor Scheme for the External Synchronization of Mutually Coupled Oscillator Systems", *J Phys Soc Jpn*, **77**, 024002, 2008.

[15] S. Nagano, "Receptors as a master key for synchronization of rhythms", *Phys Rev E*, **67**, 056215, 2003.

[16] S. Nagano, "Noise reduction and signal enhancement by receptor synchronization", NOLTA **11**, 601-609, 2020. DOI: 10.1587/nolta.11.601

[17] J. Pantaleone, "Synchronization of metronomes", *American Journal of Physics*, **70**, 992-1000, 2002.

[18] S. Nagano, "Diffusion-assisted aggregation in crystal growth", *Journal of Physics: Condensed Matter*, **10**, 11577, 1998.

[19] S. Nagano, "Ion-channel-based complete synchronization between neurons". submitted to Phys Rev E, 2023.